crystals

MDPI

Article

Dynamics–Function Correlation in Photosystem II: Molecular Dynamics in Solution

Maksym Golub [1], Miriam Koppel [2], Piret Pikma [2], Bernhard Frick [3] and Jörg Pieper [1,*]

[1] Institute of Physics, University of Tartu, 50411 Tartu, Estonia
[2] Institute of Chemistry, University of Tartu, 50411 Tartu, Estonia; piret.pikma@ut.ee (P.P.)
[3] Institute Laue-Langevin, Avenue des Martyrs 71, CEDEX 9, 38042 Grenoble, France
* Correspondence: pieper@ut.ee; Tel.: +372-737-4627

Abstract: A detailed comprehension of protein function requires information on the spatial structure of the protein, which is often gathered from X-ray crystallography. However, conformational dynamics often also plays an important functional role in proteins and can be directly investigated by complementary quasielastic neutron scattering. A classic example for dynamics–function correlations is Photosystem II, which is a multimeric pigment–protein complex responsible for catalyzing the light-induced photosynthetic water splitting into protons and oxygen. Several functional subprocesses of photosynthetic electron transfer and water splitting are strongly dependent on temperature and hydration, two factors also known to affect protein dynamics. Photosystem II is often investigated in the form of membrane fragments, where the protein complex remains embedded into its native lipid environment. However, experiments on protein function are often carried out in solution state, while direct investigations of molecular dynamics by quasielastic neutron scattering are mainly performed using specifically hydrated membrane fragments only. The present study provides the first quasielastic neutron scattering investigation of the molecular dynamics of Photosystem II membrane fragments (PSIImf) in solution over a wide temperature range from 50 to 300 K. At physiological temperatures above the melting point of water, we observed that the dynamics of PSIImf are significantly activated, leading to larger atomic mean square displacement values compared to those of specifically hydrated membrane stacks. The QENS data can be described by two dynamical components: a fast one, most probably corresponding to methyl group rotation; and a slower one, representing localized conformational dynamics. The latter component could be fitted by a jump-diffusion model at 300 K. The dynamics observed characterize the level of flexibility necessary for the proper PS II functionality under physiological conditions. In contrast, we observe a severe restriction of molecular dynamics upon freezing of the solvent below ~276 K. We associate this unexpected suppression of dynamics with a substantial aggregation of PSIImf caused by ice formation.

Keywords: photosystem II; protein dynamics; electron transfer; quasielastic neutron scattering

Citation: Golub, M.; Koppel, M.; Pikma, P.; Frick, B.; Pieper, J. Dynamics–Function Correlation in Photosystem II: Molecular Dynamics in Solution. *Crystals* **2023**, *13*, 1441. https://doi.org/10.3390/cryst13101441

Academic Editors: Rocco Caliandro and Benedetta Carrozzini

Received: 31 August 2023
Revised: 21 September 2023
Accepted: 22 September 2023
Published: 28 September 2023

1. Introduction

Photosynthesis is the fundamental physiological process by which green plants and cyanobacteria convert light energy into storable chemical energy by synthesizing glucose. As the primary energy source for nearly all ecosystems and the foundation of the food chain for numerous species, photosynthesis is a critical process for life on Earth. Photosynthesis is a multifaceted process encompassing several stages. The light-induced water splitting occurs in Photosystem II (PS II), a multi-subunit protein complex found in the thylakoid membranes of photosynthetic organisms [1]. The crystal [2] and solution structures of PSII [3] are shown in Figure 1. The redox reactions triggered by light in PS II are greatly influenced by temperature and hydration. Therefore, it is evident that the conformational dynamics of PS II play a critical role in these redox reactions, as the latter changes in dynamics with temperature, and hydration levels strongly correlate with functional processes in PS II [4].

Dynamics–function correlations have often been inferred indirectly when observing pronounced temperature dependences of functional processes. This implies that the "freezing" of conformational dynamics upon temperature decrease impairs functionally important structural changes in proteins [5]. In the case of PSII, the light-induced charge separation, leading to the formation of the radical ion pair $P680^{+\bullet}Q_A^-$, remains active even at low temperatures [6]. However, the reoxidation of this pair by the primary electron acceptor $Q_A^{-\bullet}$ by Q_B, is blocked completely below 200 K [7–9], and the individual redox steps of the water-oxidizing complex display a distinct temperature dependence (see e.g., [10]). In addition, the hydration level has a significant effect on the reoxidation of Q_A^- [11] and the redox steps of the water-oxidizing complex [12]. These effects appeared to be consistent with a reorientation of the Q_B headgroup upon electron uptake reported based on X-ray crystallography, implying a two-state gating mechanism (see Figure 1) [13]. The two orientations of the Q_B headgroup are shown in violet and cyan colors in Figure 1, respectively, and are plotted along with the neighboring protein residues shown in grey and labeled by residue number. The rearrangements also encompass the breaking and formation of hydrogen bonds. Later, however, the conformational changes required for Q_B reduction by Q_A were described as much more complex, comprising additional rearrangements of hydrogen bonds, e.g., the reorientation of the Ser223 residue in the vicinity of the Q_B binding site [14,15]. It was inferred indirectly that the presence of a general conformational flexibility of PSII is required to allow the above rearrangements of Q_B and of its protein environment upon electron transfer. In turn, a freezing of protein flexibility was assumed to inhibit electron transfer. It was also shown that a fine-tuning of protein dynamics leads to thermal adaptation of electron transfer in thermophile bacteria [16]. Therefore, understanding the correlation between protein dynamics and function is essential for a deeper comprehension of these processes. However, a direct proof of a dynamics–function correlation was still lacking.

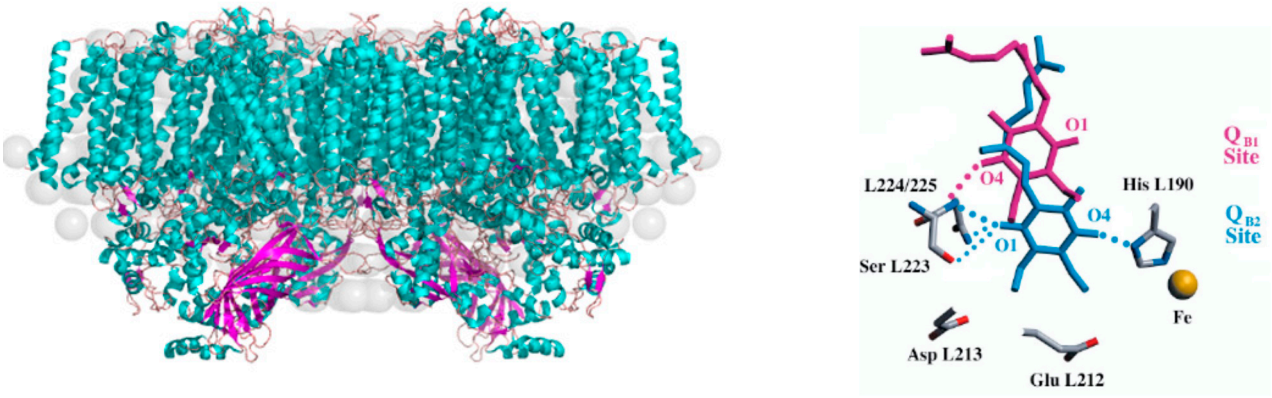

Figure 1. (**Left**): Comparison of the crystal structure of PSII of *Thermosynechococcus elongatus* (pdb 5 kaf [2]) shown in cyan and violet with the solution structure determined from SANS data (gray spheres) with the PSII crystal structure. This figure is adapted from Golub et al. [3] Copyright (2023) American Chemical Society. (**Right**): Conformational changes in the vicinity of the Q_B binding site upon $Q_A \rightarrow Q_B$ electron transfer according to Stowell et al. [13], see text. This figure is reprinted from Stowell et al. [13] with permission.

Therefore, quasielastic neutron scattering (QENS) was used to directly investigate the dynamics of hydrated PS II membrane fragments (PSIImf) from spinach [17,18]. The dynamics of PS II was studied over a temperature range of 5 to 300 K, and a dynamical transition with a strong increase of molecular mobility with increasing temperature was reported at approximately ~240 K at 90% relative humidity [18]. It was shown that the latter increase of molecular mobility is strongly correlated with the temperature-dependent increase of the electron transport efficiency from $Q_A^{-\bullet}$ to Q_B. The latter dynamics–function correlation is visible in Figure 2, where the mean square displacement $<u^2>$ (MSD) is shown

by black diamonds along with the electron transport efficiency provided by red diamonds. Between 280 and 340 K, the dynamics of PSIImf revealed a hydration-sensitive transition occurring between 310 and 320 K, which was attributed to the detachment of the oxygen-evolving complex [19]. At room temperature, the protein dynamics were suppressed below 44% r.h., which aligns with the inhibition of electron reduction in dehydrated PS II [17]. Point mutations in the vicinity of the cofactors Q_A and Q_B were shown to affect the overall protein dynamics in bacterial reaction centers [20,21].

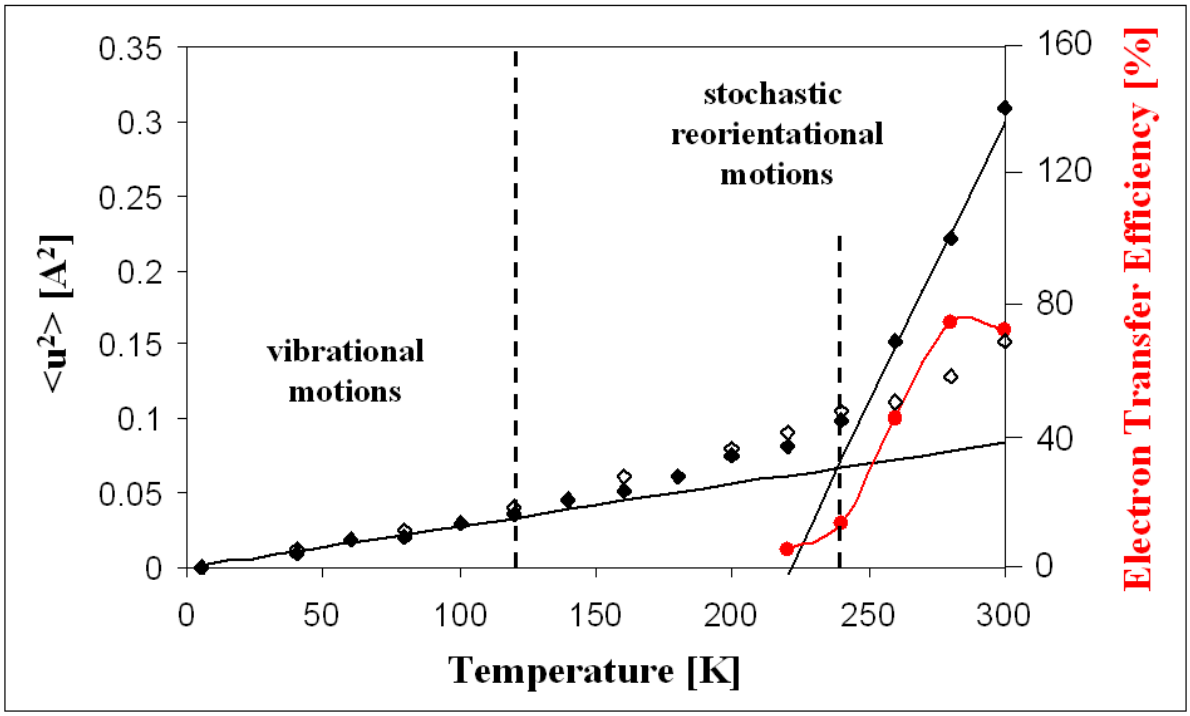

Figure 2. Temperature dependence of the average atomic mean square displacement $<u^2>$ for hydrated (full symbols) and dry PS II membrane fragments (open symbols). The red points represent the temperature dependence of the $Q_A \rightarrow Q_B$ electron transfer efficiency in PS II (left scale) This figure is adapted from data of [18]. Copyright (2007) American Chemical Society.

Therefore, exploring the correlations between protein dynamics and function is crucial for a deeper comprehension of these processes. However, previous QENS studies were largely restricted to experiments using specifically hydrated membranes to avoid a sizeable scattering contribution from the solvent. This means that a thorough examination of the conformational dynamics of PSIImf in solution, which is close to its native state, is so far lacking. QENS is a highly effective experimental technique for directly investigating protein dynamics (for more details, see [22–24]). This method takes advantage of the fact that hydrogen atoms are uniformly distributed in biomolecules and have a high scattering cross-section [22,25,26] so that they can serve as efficient probes of the overall molecular dynamics. As a result, QENS has become widely used for studying the molecular motions of proteins on the picosecond to nanosecond timescale [5].

Our study seeks to go beyond the use of hydrated membranes and to explore the dynamics of PSIImf in solution for the first time. We are presenting QENS measurements over a wide temperature range from 50 K to 295 K. As solution measurements of molecular dynamics contain contributions from both the protein/membrane and from the buffer, a reliable method for buffer subtraction is a key prerequisite for obtaining reasonable data. Below, we present such an approach based on the coherent scattering of the D_2O present in the solvent and apply it to PSIImf for the first time. As a result, we are able to directly probe the dynamics of PSIImf in solution, i.e., in the same form as routinely used for studies of functional processes in PSII by employing complementary methods of optical

spectroscopy [6–9,11,12]. In perspective, these insights will help us to achieve a direct dynamics–function correlation and a better understanding of the vital role that dynamics play in protein function.

2. Materials and Methods

Sample preparation: The preparation of PSIImf was described in detail earlier [18]. Briefly, PSIImf were isolated from spinach (*Spinacea oleracea*) following the procedure described by Berthold et al. [27]. PSIImf with modifications according to Völker et al. [28]. Finally, the PS II membrane fragment sample was prepared in a buffer solution containing D_2O, 50 mM MES (pD 6.5), 0.4 M sucrose, 15 mM NaCl, and 10 mM $CaCl_2$ at a concentration of 80 mg/mL. We used a flat cylindrical aluminum slab cell with a diameter of 50 mm and a thickness of 0.4 mm filled with 1 mL sample or buffer solution for the measurement.

QENS experiment: To measure the QENS spectra of PSIImf in a D_2O solution, we employed the IN6 time-of-flight spectrometer at ILL (Grenoble, France). The experiments were conducted using a sample cell with a cylindrical shape in a temperature range spanning from 50 K to 295 K. For accurate buffer subtraction at each temperature point, we also measured the buffer solution separately, but under the same conditions as the PSIImf. The incident neutron wavelength was 5.12 Å, which corresponded to a q-range of 0.2 to 2 Å. We estimated the elastic energy resolution to be 88 μeV based on standard vanadium measurement.

We utilized the Large Array Manipulation Program (LAMP) for the data reduction process. The raw data were normalized based on the elastic intensity of vanadium runs and corrected for detector efficiency. Finally, the scattering function $S_{exp}(Q,\omega)$ was transferred in energy and momentum transfer scale.

QENS data analysis: In the case of a protonated scatterer like a protein, the number of neutrons detected in a solid angle element $\delta\Omega$ and an energy element $\delta\omega$ in an incoherent neutrons scattering experiment is provided by the double-differential cross-section $\frac{\delta^2\sigma}{\delta\Omega\delta\omega}$ (for an overview, see, e.g., Ref. [29])

$$\frac{\delta^2\sigma}{\delta\Omega\delta\omega} = \frac{|\boldsymbol{k_1}|}{|\boldsymbol{k_0}|} b_{inc}^2 S_{inc}(Q,\omega) \tag{1}$$

where $\boldsymbol{k_0}$ and $\boldsymbol{k_1}$ are the wave vectors of the incident and scattered neutrons, respectively, Q is the momentum transfer vector, b_{inc} is the incoherent scattering length, and $S_{inc}(Q,\omega)$ is the incoherent scattering function. $S_{inc}(Q,\omega)$ is not directly accessible in experiments; it has to be replaced by the experimental scattering function $S_{exp}(Q,\omega)$, which can be provided as:

$$S_{exp}(Q,\omega) = F_N exp\left(-\frac{\hbar\omega}{2kT}\right) R(Q,\omega) \otimes S_{theo}(Q,\omega) \tag{2}$$

which consists of a normalization factor F_N, the detailed balance factor according to $exp\left(-\frac{\hbar\omega}{2kT}\right)$, the instrument resolution function $R(Q,\omega)$ and a model scattering function $S_{theo}(Q,\omega)$, which are a function of energy $\hbar\omega$ and the momentum transfer vector Q. The following model function often represents the theoretical function characterizing the dynamics of the protein:

$$S_{theo}(Q,\omega) = e^{-<u^2>Q^2}\left\{A_0(Q)\delta(\omega) + \sum_n A_n(Q)L_n(H_n,\omega) + S_{in}(Q,\omega)\right\} \tag{3}$$

which consists of the Debye–Waller factor $e^{-(u^2)Q^2}$ with the "global" vibrational mean square displacement $<u^2>$ (MSD), the elastic component $A_0(Q)\delta(\omega)$, the quasielastic component $\sum_n A_n(Q)L_n(H_n,\omega)$, and, finally, the (vibrational) inelastic contribution $S_{in}(Q,\omega)$. Assuming an exponential protein relaxation, the line shape $L_n(H_n,\omega)$ becomes a Lorentzian with a width H_n (HWHM) related to a characteristic relaxation time τ_R. The pre-factors

$A_0(Q)$ and $A_n(Q)$ are denoted as elastic and quasielastic incoherent structure factors (EISF and QISF), respectively, which add up to unity according to

$$\sum_n A_n(Q) = 1 - A_0(Q) \tag{4}$$

Elastic incoherent neutron scattering data can be analyzed in terms of the Gaussian approximation according to

$$S_{exp}(Q, \omega = 0 \pm \triangle E) \approx I_0 e^{-<u^2>Q^2} \tag{5}$$

The value of the average atomic *MSD* at a given temperature can be obtained from the slope of the semi-logarithmic plot of the elastic intensity

$$MSD = -\frac{d\ \ln\left[S_{exp}(Q, \omega = 0 \pm \triangle E)\right]}{d\ Q^2} \tag{6}$$

This approximation is valid only at $Q \to 0$, but can be extended to $MSD^* Q^2 \leq 1$ [22]. According to Equation (3), the QENS spectrum measured at 295 K was fitted using a sum of one elastic contribution and two Voigt functions as the convolution of a Lorentzian with the experimental resolution. The experimental resolution is defined according to the fit of the vanadium spectrum and has been fixed in all further fits. In the case of a jump-diffusion model of the protons' motion within the protein suggested by Singwi and Sjölander [30], the Lorentzian *HWHM* is expected to follow

$$HWHM(Q) = \frac{DQ^2}{1 + D\tau Q^2} \tag{7}$$

where τ provides the residence time, during which protons oscillate around an equilibrium position, and D is the jump-diffusion constant, which describes the diffusive motion of protons from one equilibrium position to another. Previously, the jump-diffusion model was successfully applied to describe the internal motions of proteins [24,31–33]. Fitting of the QENS spectra has been performed in OriginPro 2018 program [34].

3. Results and Discussion

Buffer subtraction: The QENS signal of a protein in solution comprises both protein and solvent contributions, thus necessitating buffer subtraction. One approach involves analyzing the coherent scattering of D_2O, which primarily originates from the buffer. Figure 3 displays the angle spectrum or diffractogram of the PS II membrane fragment sample in buffer solution (black line) and of the separate buffer measurement (red line). The sample spectrum exhibits a correlation peak at a 2θ-value of roughly 100°, similar to the peak visible in the buffer data. Note that the latter position may be affected by angle-dependent detector efficiency, but a precise determination was not within the scope of this study. The correlation peak corresponds mainly to D_2O coherent scattering and is not present for incoherent scatterers like a protein, membrane or the vanadium standard [35]. To estimate the PSIImf contribution, we followed [36], and performed buffer subtraction with a scaling factor of k. The correlation peak disappears after the subtraction, and the resulting diffractogram becomes flat, akin to the vanadium standard. In this case, the scaling factor k equals 0.9, meeting the buffer subtraction criteria. This procedure enabled us to isolate the QENS signal of PSIImf for further analysis and obtain accurate data on their dynamical behavior in solution.

Dynamics at physiological temperatures: The central aim of this investigation is to explore the conformational dynamics of PSIImf in solution under physiological temperature conditions. We first measured QENS spectra of PSIImf at 295 K (see Figure 4A). In the latter spectrum, the broadening that is visible around the elastic peak is generally associated with diffusive conformational motions between different protein conformations on the

picosecond timescale. These motions are deemed to be an essential component of the functional structural changes necessary for the functional processes [17,37,38].

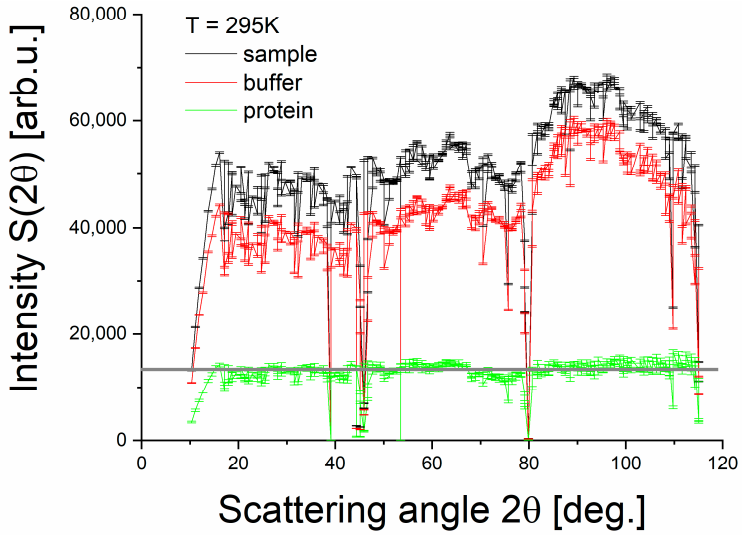

Figure 3. Buffer subtraction for the case of the PS II membrane fragment sample at 295 K: Angle spectra (diffractograms) of PS II in buffer solution (black line), a separate buffer sample (red line). Each data point is scattering intensity at a specific angle averaged over all neutron energies. The PS II contribution (green line) is obtained by subtracting the buffer signal from the sample data under the condition that the coherent peak at about 100° vanishes. As a result, the PS II contribution is virtually featureless, as expected for an incoherent scatterer (see flat gray guiding line). The scaling factor to subtract the buffer is found to be 0.9.

We further analyzed the PSIImf QENS spectra collected at 295 K by utilizing model scattering functions (as outlined in Equations (2) and (3)) in the energy range of −2 meV to 2 meV. The fit obtained (as illustrated in Figure 4A by the red line) is the summation of a Gaussian peak representing the elastic contribution and of two quasielastic Voigt peaks corresponding to the fast (for broader linewidth) and the slow (for narrow linewidth) components of the protein dynamics, respectively. It has to be kept in mind that this is a minimal description of the measured QENS data, so that each of the two components represents a larger number of unresolved motional components expected in the accessible observation time range.

The Lorentzian linewidths of the QENS spectra are sensitive to the wavevector Q, which enables the differentiation and characterization of various motions within the protein system being studied. The broader quasielastic peak that represents the fast motions (depicted by the dotted line in Figure 4A) exhibits a constant Lorentzian HWHM, indicating a fast rotational motion. Through several fitting iterations, we identified an optimal Lorentzian HWHM of approximately 1.1 ± 0.2 meV, which corresponds to a rotation frequency of 1.67 ps^{-1}. Similarly, fast dynamical contributions were associated, e.g., with the rotation of the CH_3 groups [39,40]. Another possible interpretation of the broad QENS component may lie in even faster motions corresponding to hydrogen atoms engaging in swift, non-oscillatory librational movements around the carbon atom they are bonded to [41]. The narrower quasielastic contribution corresponds to slower motions that we associate with internal protein dynamics (as indicated by the blue dashed line in Figure 4A). For this dynamical component, we observed a Q-dependence of the HWHM that follows the typical behavior of a localized jump-diffusion (as shown in Figure 4B). The jump-diffusion model has been previously used to describe the internal motions of proteins in various studies [24,31,33,42]. Through our analysis, we determined a diffusion coefficient of 4.4 ± 0.5 10^{-9} m^2/s and a residence time of 3.2 ± 0.5 ps.

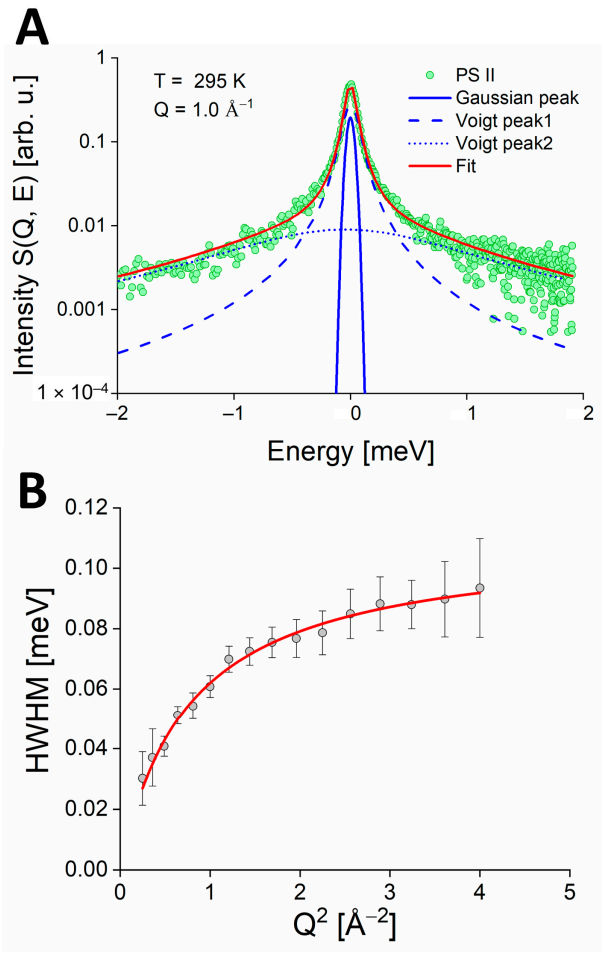

Figure 4. (**A**): Fit example of PS II QENS spectrum (green points), collected at Q of 1.0 Å^{-1} at IN6 at 295 K. The solid blue line represents the elastic component; the blue dashed line corresponds to the slow internal dynamics; the blue dotted line to fast rotational motions. The solid red line represents the final fit. (**B**): HWHMs obtained from the fit of the QENS spectra for the slow internal dynamics (see the blue dash line in panel A. HWHMs of PSIImf are represented as gray circles. The red line represents the fit by the jump-diffusion model (see Equation (7)).

Temperature dependence of molecular dynamics: Our subsequent aim was to examine the temperature dependence of MSDs for PSIImf in solution based on the elastic intensity using Equation (6). To define the EINS intensity from the measured $S_{exp}(Q,\omega)$ data, we utilized the ElasticWindow algorithm (Elwin), which is implemented in the Mantid program. In this approach, we considered a region of elastic intensity that corresponded to the energy range of −0.12 to 0.12 meV for the IN6 instrument (as shown in Figure 5A). The "elastic" slice was estimated as the integrated intensity within the aforementioned elastic energy window (represented by the green points in Figure 5B). One has to consider the quasielastic contribution that is not neglectable in the elastic window at higher q values (see Figure 4A), which is specifically the case for data taken at temperatures above ice melting point. We took the quasielastic background to EINS intensity (indicated by black points in Figure 5B) into account by integrating the scattering intensity in the energy range from −0.36 to −0.12 meV (as illustrated in Figure 5A). Finally, we estimated the EINS intensity by subtracting the intensity of the "quasielastic" slice from that of the "elastic" slice (as indicated by the red point in Figure 5B). This analysis was repeated for EINS data at each measured temperature. Figure 6 shows EINS for the temperature point of 295 K obtained according to the Elwin approach (see red points) and EINS estimated from the Q-dependent analysis, i.e., without considering the quasielastic contribution (see open diamonds). A comparison of the MSDs determined by both approaches reveals that the

Elwin method leads to larger MSDs because of a more realistic estimate of the elastic intensity (see Figure 7).

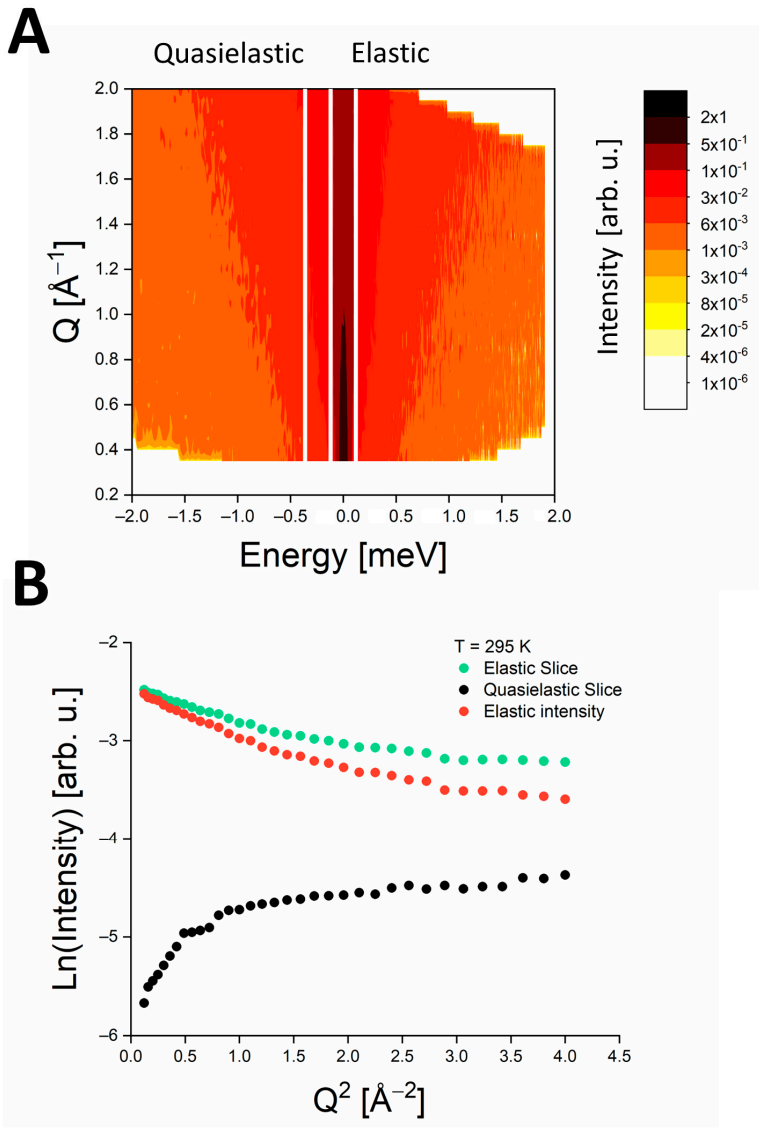

Figure 5. (**A**) $S_{exp}(Q,\omega)$ data of PSIImf at T = 295 K. White vertical lines define "elastic" and "quasielastic" slices that correspond to energy ranges from −0.12 to 0.12 meV and from −0.36 to −0.12 meV, respectively. (**B**) Example of EINS data at T = 295 K. Green data points denote the integrated intensity inside the elastic region in panel (**A**). The black points show the integrated intensity inside the energy region defined as the "quasielastic" slice in panel (**A**). Finally, EINS data (red points) are obtained as a difference between integrated intensities of the "elastic" and "quasielastic" slices, respectively.

The MSDs are determined from the EINS data according to Equation (6). The fit range was restricted to the Q values between 0.12 and 1.21 Å^{-1}, where the dependence of ln $[S(Q,\omega = 0 \pm \Delta E)]$ on Q^2 was found to be linear within the experimental uncertainty (see Figure 6). The temperature dependence of the *MSD* values is shown in Figure 7 (red points). For comparison, we also show MSDs of PSIImf measured previously in dry state and at 90% relative humidity (r.h.) [18], see green and blue points in Figure 7, respectively.

As visible in Figure 7, the *MSD* values for PSIImf in solution above the melting point of D_2O are significantly higher than those obtained earlier for hydrated membrane stacks. In contrast, however, the MSDs in solution state appear to be significantly suppressed at lower temperatures, with the latter surprising observation especially requiring a discussion.

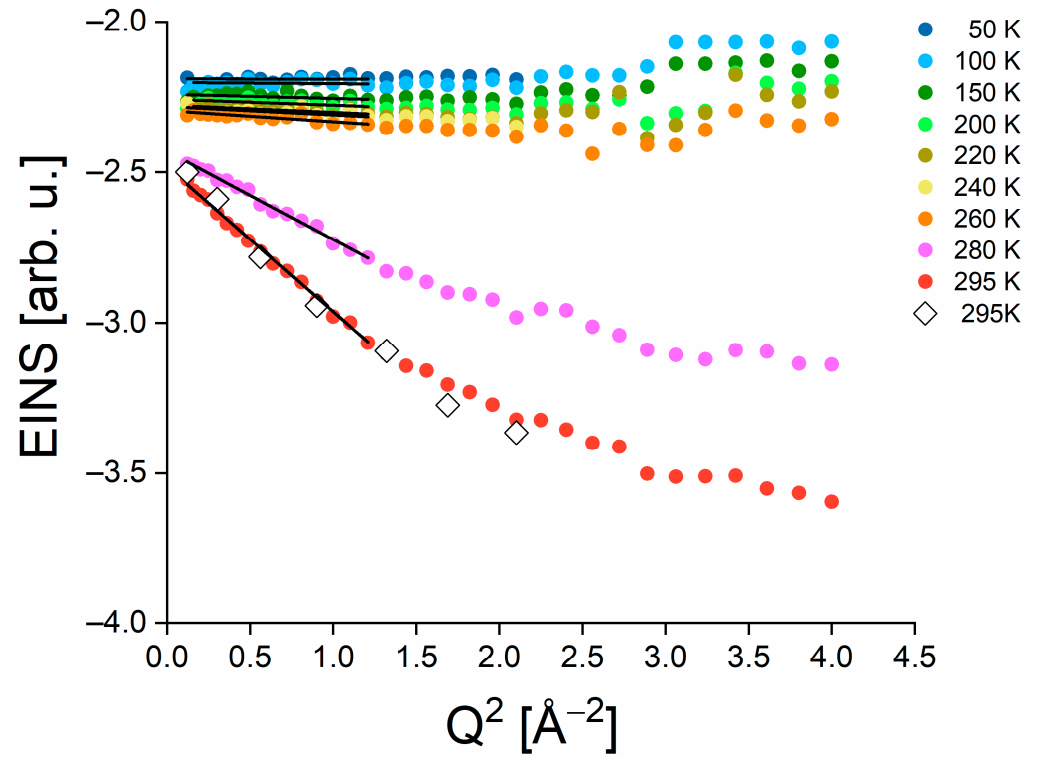

Figure 6. Full points represent semi-logarithmic plots of EINS data plotted against Q^2 to estimate $\langle u^2 \rangle$ at different temperature points taking into account the quasielastic contribution. Black lines denote the linear fits in the Q^2 range from 0.12–1.21 Å^{-2}. The open diamonds correspond to EINS obtained solely from the data at the elastic slice at 295 K, as shown in Figure 5B.

Starting from previously published data, the MSDs for PSIImf hydrated at 90% r.h. reveal a notable increase in molecular dynamics in the temperature above 230 K (see dotted blue guiding line in Figure 7). The latter effect was referred to as the dynamical transition in proteins [43], membranes [37,44], and model membrane systems [45] and associated with the onset of diffusive conformational dynamics. Similar effects were observed for PSII [46], and other photosynthetic proteins [47]. It has to be noted, however, that the presence of a dynamical transition as such has been questioned (see, e.g., Ref. [48]). The latter study of the dynamics of lysozyme combining QENS and dielectric spectroscopy suggests that there is no specific transition at 230 K, but rather a thermal activation of molecular dynamics, whose relaxation time enters the observation time window of the spectrometer at a specific temperature. Regardless of the latter question, however, the temperature dependence of electron transfer efficiency appears to be correlated with the thermally activated increase in protein dynamics as shown in Figure 2, thus pointing to a dynamics–function correlation in PSIImf.

As to the hydration dependence, the *MSD* values for dry PSIImf do not exhibit a similar increase in dynamics as observed for hydrated PSIImf. It was shown, especially, that the MSDs of PSIImf above 230 K increase with increasing hydration level [17]. Therefore, it should be expected that the MSDs of PSIImf in solution are generally higher than in the case of hydrated membrane stacks. This anticipated increase of protein flexibility of PSIImf in solution is indeed observed above the melting point of D_2O, thus permitting studies of molecular dynamics in solution state at physiological temperatures.

The increase in slope of the MSDs of PSIImf at 90% r.h. above roughly 130 K is often interpreted as the onset of internal protein motions, especially those of methyl groups [40,49]. In the case of the Light-Harvesting Complex II, this transition was associated with the onset of anharmonic vibrational motions [47]. The MSDs of dry PSIImf exhibit the latter transition at a slightly elevated temperature of about 200 K. Because of the above-

mentioned suppression of MSDs below the freezing point of D_2O, the latter intermediate transition cannot be detected for PSIImf in solution. That is, only two strikingly distinct temperature ranges are observed characterizing the dynamics of PSIImf in solution.

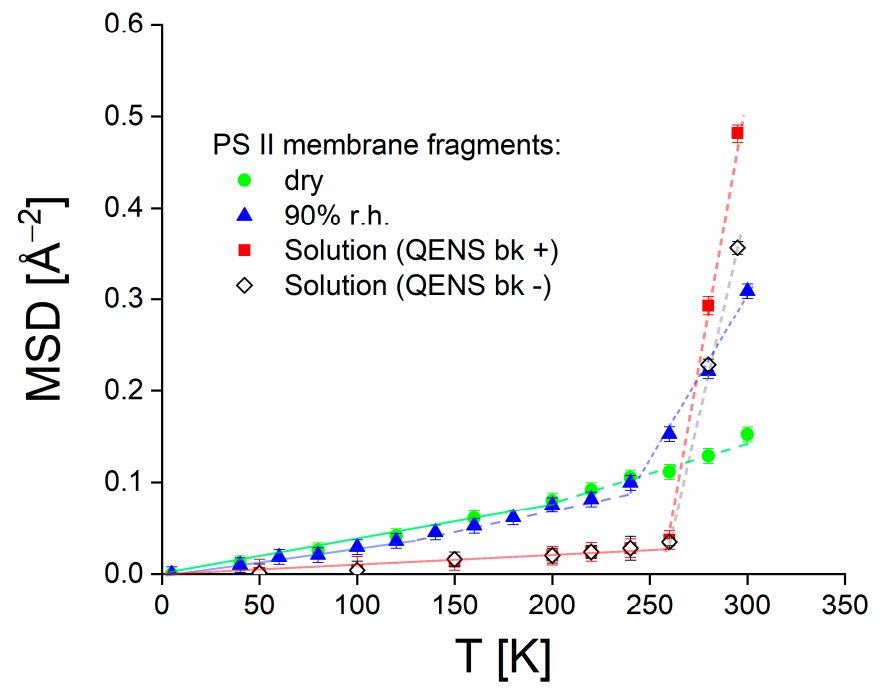

Figure 7. Temperature dependence of MSDs. Red points correspond to the MSD values obtained from the analysis shown in Figure 6 for PSIImf in solution when the quasielastic contribution is considered and subtracted. For comparison, open diamonds represent the case where EINS is taken only as the integrated intensity of the elastic slice (see Figur 5A). Received MSDs compared with MSDs of dry PSIImf (green points) and PSIImf hydrated at 90% r.h. (blue points). Solid green, blue, and red lines are for illustrative purpose. The data of dry PSIImf (green points) and PSIImf hydrated at 90% r.h. (blue points) are taken from [18] with permission.

A remarkable finding is that the *MSD* values for PSIImf in solution were significantly lower than for hydrated membranes in the temperature range below ~276 K. This temperature dependence of *MSD* was unexpected, as PSIImf in solution are generally anticipated to exhibit higher flexibility due to a higher hydration level, see above. Interestingly, SANS studies of lysozyme protein solutions reported significant protein aggregation due to ice formation below the freezing point of water [50,51]. The frozen state of the protein solution has been characterized as primarily consisting of ice crystals with regions of amorphous water containing freeze-concentrated protein. Based on the observations of Curtis et al. [50,51], we assume that a similar structural rearrangement may occur in PSIImf upon freezing, thus leading to ice-induced crowding or even unspecific aggregation. Due to the large size of the membrane fragments studied here, this effect should be even more significant than for the globular protein lysozyme. Such experiments on PSIImf in solution are planned. Crowding effects have been shown to restrict protein dynamics [52]. Therefore, we propose that the low *MSD* values corresponding to unexpectedly rigid PSIImf in solution at temperatures below ~276 K can be attributed to the restriction of protein dynamics due to ice-induced aggregation. This result suggests that the influence of dynamic restriction due to aggregation in ice overpowers the occurrence of a classical dynamic transition. Further investigation into the dynamic transition of PSIImf in solution may involve utilizing cryoprotectants, such as glycerol, to prevent ice formation. However, conducting such experiments is beyond the scope of the present work.

4. Conclusions

This study provides a comprehensive analysis of the dynamical behavior of PSIImf in solution and elucidates two distinct temperature regions of molecular dynamics. Specifically, our investigation characterizes the flexibility of PSIImf in a native liquid state at physiological temperatures.

In summary, we observed that the dynamics of PSIImf are significantly activated at temperatures above the melting point of water, leading to larger *MSD* values compared to those of specifically hydrated membrane stacks. In this temperature regime, the *MSD* values for PSIImf in solution are up to twice as high as for the hydrated membrane stacks as expected for a higher hydration level. A jump-diffusion model has been used to characterize the time scale of this conformational dynamics at the temperature of 295 K. The obtained results characterize the level of flexibility necessary for the proper PS II functionality under physiological conditions, which plays a vital role in photosynthetic water splitting to generate oxygen. To perform these essential functions, PS II requires structural flexibility, allowing the protein to undergo conformational changes necessary for electron transfer and specific steps of water splitting. In contrast, we observe a severe restriction of molecular dynamics upon freezing of the solvent below ~276 K. We associate this unexpected suppression of dynamics with a substantial aggregation of PSIImf caused by ice formation. Upon aggregation, the motional freedom of the protein becomes seriously restricted by congestion with neighboring molecules, which results in a suppression of the observed *MSD*.

Overall, this study provides valuable insights into the mechanisms of photosynthesis by highlighting the vital role that dynamics play in protein function. Understanding the dynamic processes of PSIImf in solution is essential for developing effective strategies to maintain the stability and functionality of photosynthetic organisms.

Author Contributions: Conceptualization, J.P.; methodology, B.F.; formal analysis, M.G. and M.K.; investigation, M.G., M.K., P.P. and J.P.; resources, B.F.; writing—original draft preparation, M.G. and J.P.; writing—review and editing, M.K. and P.P.; supervision, M.G. and J.P.; project administration, P.P.; funding acquisition, J.P. All authors have read and agreed to the published version of the manuscript.

Funding: This research was funded by the Estonian Research Council (Grants PRG 539 and PRG676) and by the Estonian Ministry of Education and Research through funding from SLTKT16432T.

Institutional Review Board Statement: Not applicable.

Informed Consent Statement: Not applicable.

Data Availability Statement: The data presented in this study are openly available at https://doi.ill.fr/10.5291/ILL-DATA.8-04-734 (accessed on 1 September 2023).

Acknowledgments: Financial support by the Estonian Research Council (Grant PRG 539) is gratefully acknowledged. This research was partially supported by the EU through the European Regional Development Fund (Centers of Excellence, TK141 "Advanced materials and high-technology devices for sustainable energetics, sensorics and nanoelectronics"), by the Estonian Ministry of Education and Research through funding from SLTKT16432T "Estonian participation in designing, construction and application of the ESS 1.09.2015–31.08.2023)", as well as by the Estonian Research Council through grant PRG676. Finally, we thank the ILL (Grenoble, France) for the allocation of beamtime at the instrument IN6 (DOI: 10.5291/ILL-DATA.8-04-734).

Conflicts of Interest: The authors declare no conflict of interest.

References

1. Ke, B. *Photosynthesis: Photobiochemistry and Photobiophysics*; Kluwer Academic Publisher: Dordrecht, The Netherlands, 2001; Volume 10.
2. Young, I.D.; Ibrahim, M.; Chatterjee, R.; Gul, S.; Fuller, F.; Koroidov, S.; Brewster, A.S.; Tran, R.; Alonso-Mori, R.; Kroll, T.; et al. Structure of Photosystem II and Substrate Binding at Room Temperature. *Nature* **2016**, *540*, 453–457. [CrossRef]

3. Golub, M.; Gätcke, J.; Subramanian, S.; Kölsch, A.; Darwish, T.; Howard, J.K.; Feoktystov, A.; Matsarskaia, O.; Martel, A.; Porcar, L.; et al. "Invisible" Detergents Enable a Reliable Determination of Solution Structures of Native Photosystems by Small-Angle Neutron Scattering. *J. Phys. Chem. B* **2022**, *126*, 2824–2833. [CrossRef]
4. Renger, G. Mechanism of Light Induced Water Splitting in Photosystem II of Oxygen Evolving Photosynthetic Organisms. *Biochim. Biophys. Acta* **2012**, *1817*, 1164–1176. [CrossRef]
5. Henzler-Wildman, K.A.; Lei, M.; Thai, V.; Kerns, S.J.; Karplus, M.; Kern, D. A Hierarchy of Timescales in Protein Dynamics Is Linked to Enzyme Catalysis. *Nature* **2007**, *450*, 913–916. [CrossRef]
6. Hughes, J.L.; Smith, P.; Pace, R.; Krausz, E. Charge Separation in Photosystem II Core Complexes Induced by 690–730 Nm Excitation at 1.7 K. *Biochim. Biophys. Acta* **2006**, *1757*, 841–851. [CrossRef]
7. Joliot, P.; Joliot, A. Different Types of Quenching Involved in Photosystem II Centers. *Biochim. Et Biophys. Acta* **1973**, *305*, 202–216. [CrossRef]
8. Renger, G.; Gleiter, H.M.; Haag, E.; Reifarth, F. Photosystem-II—Thermodynamics and Kinetics of Electron-Transport from Q(a)(-) to Q(B)(Q(B)(-)) and Deleterious Effects of Copper(II). *Z. Naturforsch.* **1993**, *48*, 234–240. [CrossRef]
9. Garbers, A.; Reifarth, F.; Kurreck, J.; Renger, G.; Parak, F. Correlation between Protein Flexibility and Electron Transfer from Qa-* to Qb in PSII Membrane Fragments from Spinach. *Biochemistry* **1998**, *37*, 11399–11404. [CrossRef]
10. Renger, G. Coupling of Electron and Proton Transfer in Oxidative Water Cleavage in Photosynthesis. *Biochim. Biophys. Acta* **2004**, *1655*, 195–204. [CrossRef]
11. Kaminskaya, O.; Renger, G.; Shuvalov, V.A. Effect of Dehydration on Light-Induced Reactions in Photosystem II: Photoreactions of Cytochrome B559. *Biochemistry* **2003**, *42*, 8119–8132. [CrossRef]
12. Noguchi, T.; Sugiura, M. Ftir Detection of Water Reactions During the Flash-Induced S-State Cycle of the Photosynthetic Water-Oxidizing Complex. *Biochemistry* **2002**, *41*, 15706–15712. [CrossRef]
13. Stowell, M.H.; McPhillips, T.M.; Rees, D.C.; Soltis, S.M.; Abresch, E.; Feher, G. Light-Induced Structural Changes in Photosynthetic Reaction Center: Implications for Mechanism of Electron-Proton Transfer. *Science* **1997**, *276*, 812–816. [CrossRef]
14. Baxter, R.H.; Ponomarenko, N.; Srajer, V.; Pahl, R.; Moffat, K.; Norris, J.R. Time-Resolved Crystallographic Studies of Light-Induced Structural Changes in the Photosynthetic Reaction Center. *Proc. Natl. Acad. Sci. USA* **2004**, *101*, 5982–5987. [CrossRef]
15. Mulkidjanian, A.Y.; Kozlova, M.A.; Cherepanov, D.A. Ubiquinone Reduction in the Photosynthetic Reaction Centre of Rhodobacter Sphaeroides: Interplay between Electron Transfer, Proton Binding and Flips of the Quinone Ring. *Biochem. Soc. Trans.* **2005**, *33*, 845–850. [CrossRef]
16. Shlyk-Kerner, O.; Samish, I.; Kaftan, D.; Holland, N.; Sai, P.S.; Kless, H.; Scherz, A. Protein Flexibility Acclimatizes Photosynthetic Energy Conversion to the Ambient Temperature. *Nature* **2006**, *442*, 827–830. [CrossRef]
17. Pieper, J.; Hauss, T.; Buchsteiner, A.; Renger, G. The Effect of Hydration on Protein Flexibility in Photosystem II of Green Plants Studied by Quasielastic Neutron Scattering. *Eur. Biophys. J. EBJ* **2008**, *37*, 657–663. [CrossRef]
18. Pieper, J.; Hauss, T.; Buchsteiner, A.; Baczynski, K.; Adamiak, K.; Lechner, R.E.; Renger, G. Temperature- and Hydration-Dependent Protein Dynamics in Photosystem II of Green Plants Studied by Quasielastic Neutron Scattering. *Biochemistry* **2007**, *46*, 11398–11409. [CrossRef]
19. Nagy, G.; Unnep, R.; Zsiros, O.; Tokutsu, R.; Takizawa, K.; Porcar, L.; Moyet, L.; Petroutsos, D.; Garab, G.; Finazzi, G.; et al. Chloroplast Remodeling During State Transitions in Chlamydomonas Reinhardtii as Revealed by Noninvasive Techniques in Vivo. *Proc. Natl. Acad. Sci. USA* **2014**, *111*, 5042–5047. [CrossRef]
20. Sacquin-Mora, S.; Sebban, P.; Derrien, V.; Frick, B.; Lavery, R.; Alba-Simionesco, C. Probing the Flexibility of the Bacterial Reaction Center: The Wild-Type Protein Is More Rigid Than Two Site-Specific Mutants. *Biochemistry* **2007**, *46*, 14960–14968. [CrossRef]
21. Russo, D.; Lambreva, M.D.; Simionesco, C.A.; Sebban, P.; Rea, G. Dynamics Properties of Photosynthetic Microorganisms Probed by Incoherent Neutron Scattering. *Biophys. J.* **2019**, *116*, 1759–1768. [CrossRef]
22. Gabel, F.; Bicout, D.; Lehnert, U.; Tehei, M.; Weik, M.; Zaccai, G. Protein Dynamics Studied by Neutron Scattering. *Q. Rev. Biophys.* **2002**, *35*, 327–367. [CrossRef] [PubMed]
23. Vural, D.; Hu, X.; Lindner, B.; Jain, N.; Miao, Y.; Cheng, X.; Liu, Z.; Hong, L.; Smith, J.C. Quasielastic Neutron Scattering in Biology: Theory and Applications. *Biochem. Biophys. Acta* **2017**, *1861*, 3638–3650. [CrossRef] [PubMed]
24. Grimaldo, M.; Roosen-Runge, F.; Zhang, F.; Schreiber, F.; Seydel, T. Dynamics of Proteins in Solution. *Q. Rev. Biophys.* **2019**, *52*, 1–63. [CrossRef]
25. Smith, J.C. Protein Dynamics—Comparison of Simulations with Inelastic Neutron-Scattering Experiments. *Q. Rev. Biophys.* **1991**, *24*, 227–291. [CrossRef] [PubMed]
26. Kneller, G.R. Quasielastic Neutron Scattering and Relaxation Processes in Proteins: Analytical and Simulation-Based Models. *Phys. Chem. Chem. Phys.* **2005**, *7*, 2641–2655. [CrossRef] [PubMed]
27. Berthold, D.A.; Babcock, G.T.; Yocum, C.F. A Highly Resolved, Oxygen-Evolving Photosystem II Preparation from Spinach Thylakoid Membranes: Epr and Electron-Transport Properties. *FEBS Lett.* **1981**, *138*, 231–234. [CrossRef]
28. Völker, M.; Ono, T.; Inoue, Y.; Renger, G. Effect of Trypsin on Ps-II Particles—Correlation between Hill-Activity, Mn-Abundance and Peptide Pattern. *Biochim. Biophys. Acta* **1985**, *806*, 25–34. [CrossRef]
29. Bee, M. *Quasielastic Neutron Scattering: Principles and Applications in Solid State Chemistry, Biological Materials Science*; CRC Press: Bristol, UK, 1988.
30. Singwi, K.S.; Sjölander, A. Diffusive Motions in Water and Cold Neutron Scattering*. *Phys. Rev.* **1960**, *119*, 863–871. [CrossRef]

31. Stadler, A.M.; van Eijck, L.; Demmel, F.; Artmann, G. Macromolecular Dynamics in Red Blood Cells Investigated Using Neutron Spectroscopy. *J. R. Soc. Interface* **2011**, *8*, 590–600. [CrossRef]
32. Stadler, A.M.; Garvey, C.J.; Embs, J.P.; Koza, M.M.; Unruh, T.; Artmann, G.; Zaccai, G. Picosecond Dynamics in Haemoglobin from Different Species: A Quasielastic Neutron Scattering Study. *Biochim. Biophys. Acta* **2014**, *1840*, 2989–2999. [CrossRef]
33. Grimaldo, M.; Roosen-Runge, F.; Hennig, M.; Zanini, F.; Zhang, F.; Jalarvo, N.; Zamponi, M.; Schreiber, F.; Seydel, T. Hierarchical Molecular Dynamics of Bovine Serum Albumin in Concentrated Aqueous Solution Below and above Thermal Denaturation. *Phys. Chem. Chem. Phys.* **2015**, *17*, 4645–4655. [CrossRef] [PubMed]
34. OriginLab Corporation. *Originpro 2018*; OriginLab Corporation: Northampton, MA, USA, 2018.
35. Gaspar, A.M.; Appavou, M.S.; Busch, S.; Unruh, T.; Doster, W. Dynamics of Well-Folded and Aatively Disordered Proteins in Solution: A Time-of-Flight Neutron Scattering Study. *Eur. Biophys. J. EBJ* **2008**, *37*, 573–582. [CrossRef]
36. Golub, M.; Moldenhauer, M.; Schmitt, F.J.; Lohstroh, W.; Maksimov, E.G.; Friedrich, T.; Pieper, J. Solution Structure and Conformational Flexibility in the Active State of the Orange Carotenoid Protein. Part II: Quasielastic Neutron Scattering. *J. Phys. Chem. B* **2019**, *123*, 9536–9545. [CrossRef] [PubMed]
37. Fitter, J.; Lechner, R.E.; Dencher, N.A. Interactions of Hydration Water and Biological Membranes Studied by Neutron Scattering. *J. Phys. Chem. B* **1999**, *103*, 8036–8050. [CrossRef]
38. Frauenfelder, H.; Chen, G.; Berendzen, J.; Fenimore, P.W.; Jansson, H.; McMahon, B.H.; Stroe, I.R.; Swenson, J.; Young, R.D. A Unified Model of Protein Dynamic. *Proc. Natl. Acad. Sci. USA* **2009**, *106*, 5129–5134. [CrossRef] [PubMed]
39. Roh, J.H.; Curtis, J.E.; Azzam, S.; Novikov, V.N.; Peral, I.; Chowdhuri, Z.; Gregory, R.B.; Sokolov, A.P. Influence of Hydration on the Dynamics of Lysozyme. *Biophys. J.* **2006**, *91*, 2573–2588. [CrossRef]
40. Schiro, G.; Caronna, C.; Natali, F.; Cupane, A. Direct Evidence of the Amino Acid Side Chain and Backbone Contributions to Protein Anharmonicity. *J. Am. Chem. Soc.* **2010**, *132*, 1371–1376. [CrossRef]
41. Wanderlingh, U.; D'Angelo, G.; Branca, C.; Nibali, V.C.; Trimarchi, A.; Rifici, S.; Finocchiaro, D.; Crupi, C.; Ollivier, J.; Middendorf, H.D. Multi-Component Modeling of Quasielastic Neutron Scattering from Phospholipid Membranes. *J. Chem. Phys.* **2014**, *140*, 174901. [CrossRef] [PubMed]
42. Stadler, A.M.; Knieps-Grunhagen, E.; Bocola, M.; Lohstroh, W.; Zamponi, M.; Krauss, U. Photoactivation Reduces Side-Chain Dynamics of a Lov Photoreceptor. *Biophys. J.* **2016**, *110*, 1064–1074. [CrossRef]
43. Doster, W.; Cusack, S.; Petry, W. Dynamical Transition of Myoglobin Revealed by Inelastic Neutron Scattering. *Nature* **1989**, *337*, 754–756. [CrossRef]
44. Lehnert, U.; Reat, V.; Weik, M.; Zaccai, G.; Pfister, C. Thermal Motions in Bacteriorhodopsin at Different Hydration Levels Studied by Neutron Scattering: Correlation with Kinetics and Light-Induced Conformational Changes. *Biophys. J.* **1998**, *75*, 1945–1952. [CrossRef]
45. Aoun, B.; Pellegrini, E.; Trapp, M.; Natali, F.; Cantu, L.; Brocca, P.; Gerelli, Y.; Deme, B.; Marek Koza, M.; Johnson, M.; et al. Direct Comparison of Elastic Incoherent Neutron Scattering Experiments with Molecular Dynamics Simulations of Dmpc Phase Transitions. *Eur. Phys. J. E Soft Matter Biol. Phys.* **2016**, *39*, 48. [CrossRef] [PubMed]
46. Pieper, J.; Trapp, M.; Skomorokhov, A.; Natkaniec, I.; Peters, J.; Renger, G. Temperature-Dependent Vibrational and Conformational Dynamics of Photosystem II Membrane Fragments from Spinach Investigated by Elastic and Inelastic Neutron Scattering. *Biochem. Biophys. Acta* **2012**, *1817*, 1213–1219. [CrossRef] [PubMed]
47. Golub, M.; Rusevich, L.; Irrgang, K.D.; Pieper, J. Rigid Versus Flexible Protein Matrix: Light-Harvesting Complex II Exhibits a Temperature-Dependent Phonon Spectral Density. *J. Phys. Chem. B* **2018**, *122*, 7111–7121. [CrossRef] [PubMed]
48. Khodadadi, S.; Pawlus, S.; Sokolov, A.P. Influence of Hydration on Protein Dynamics: Combining Dielectric and Neutron Scattering Spectroscopy Data. *J. Phys. Chem. B* **2008**, *112*, 14273–14280. [CrossRef]
49. Roh, J.H.; Novikov, V.N.; Gregory, R.B.; Curtis, J.E.; Chowdhuri, Z.; Sokolov, A.P. Onsets of Anharmonicity in Protein Dynamics. *Phys. Rev. Lett.* **2005**, *95*, 038101. [CrossRef]
50. Curtis, J.E.; McAuley, A.; Nanda, H.; Krueger, S. Protein Structure and Interactions in the Solid State Studied by Small-Angle Neutron Scattering. *Faraday Discuss.* **2012**, *158*, 285–299; discussion 351–270. [CrossRef]
51. Curtis, J.E.; Nanda, H.; Khodadadi, S.; Cicerone, M.; Lee, H.J.; McAuley, A.; Krueger, S. Small-Angle Neutron Scattering Study of Protein Crowding in Liquid and Solid Phases: Lysozyme in Aqueous Solution, Frozen Solution, and Carbohydrate Powders. *J. Phys. Chem. B* **2012**, *116*, 9653–9667. [CrossRef]
52. Roosen-Runge, F.; Hennig, M.; Zhang, F.; Jacobs, R.M.; Sztucki, M.; Schober, H.; Seydel, T.; Schreiber, F. Protein Self-Diffusion in Crowded Solutions. *Proc. Natl. Acad. Sci. USA* **2011**, *108*, 11815–11820. [CrossRef]